The Effect of α-Al_2O_3 Composite on Energy Storage Characteristics of the Orthogonal Phase PLZST Antiferroelectric Ceramics

Yuzhe Chen
University of Electronic Science and Technology of China
Hongwei Chen (hwchen@uestc.edu.cn)
University of Electronic Science and Technology of China
Libin Gao
University of Electronic Science and Technology of China
Kexin Liang
University of Electronic Science and Technology of China
Zhiqiang Wang
University of Electronic Science and Technology of China
Jihua Zhang
University of Electronic Science and Technology of China

Research Article

Keywords: Al2O3, PLZST, Energy storage, Breakdown strength

Posted Date: December 7th, 2021

DOI: https://doi.org/10.21203/rs.3.rs-1123469/v1

Abstract

The effect of (1-x)($Pb_{0.97}La_{0.02}$)($Zr_{0.675}Sn_{0.285}Ti_{0.04}$)$O_3$-x$Al_2O_3$, with x=0~0.04, 0.08, 0.10 composite ceramic samples was studied. In this experiment, the PLZST powder was pre-fired to obtain the perovskite structure, and then combined with α-Al_2O_3 to increase the BDS of the ceramic. The test results show that the composite thick film samples are all perovskite orthorhombic phases, and Al_2O_3 is mainly filled in the grain gaps with a flaky structure. A proper content of composite Al_2O_3 can increase the density of ceramics. With x=0.02, the maximum value of BDS is 25.27 kV/mm, which is 60% higher than pure PLZST material, and the releasable energy storage density also reaches a maximum of 2.95 J/cm³. After the composite amount exceeds 0.03, the saturation polarization intensity decreases significantly. The energy storage efficiency of each sample is generally not high, all of which are less than 65%.

1. Introduction

Rapidly growing demand for related development of pulsed power applications and modern electronics put forward higher requirements for the performance of the energy storage capacitor[1–5]. Among these energy storage capacitors, dielectric capacitors have the highest power densities on account of their ultrafast charging/discharging rates (<1μs). In addition, it has a high range of use, lower cost and higher life expectancy [6, 7]. Recently, the ($Pb_{1-x}La_x$) ($Zr_ySn_zTi_{1-y-z}$) O_3 (PLZST) materials as a branch of dielectric materials attract much attention. PLZST, as a typical antiferroelectric ceramic material, has two phases: the antiferroelectric phase and the ferroelectric phase. Crystal phase transformation occurs when the electric field exceeds a certain intensity. Thus, it has double hysteresis loop, the high saturation polarization and nearly zero remnant polarization[8–16]. It becomes an excellent candidate for high density energy storage capacitors.

Universally, the phase transition field of orthogonal perovskite phase is large (20 kV/mm). Many orthogonal ceramic samples of different components have been broken down before phase transformation under the action of applied electric field. It is known that the dielectric breakdown strength of ceramic materials has a strong dependence on the grain size, with smaller grains giving higher dielectric breakdown strength (BDS)[17–21]. α-Al_2O_3, as a superior dielectric material, possesses a high breakdown strength (300–700 kV/mm) and high band gap (~9 eV) in conjunction with its excellent chemical and thermal properties[22]. Thus, Al_2O_3 is a promising additive to achieve the intention of breakdown strength enhancement.

PLZST powder was used to obtain preliminary perovskite structure, and then composite with α-Al_2O_3 to increase the BDS of ceramics. High BDS, low dielectric loss at high frequency and high thermal stability of antiferroelectric ceramic composite Al_2O_3 are expected to be obtained. In this paper, the structure, dielectric properties, ferroelectricity and energy storage behavior of (1-x) PLZST–xAl_2O_3 (x = 0.0-0.1) system were investigated. The research mainly focused on the increase of the BDS and energy storage ability by doping Al_2O_3 in PLZST.

2. Experiment Procedure

The conventional solid-state reaction was used to prepare the ceramics of (1-x) $(Pb_{0.97}La_{0.02})(Zr_{0.675}Sn_{0.285}Ti_{0.04})O_3$-$xAl_2O_3$, with x=0~0.04, 0.08, 0.10. The PLZST raw materials PbO, La_2O_3, ZrO_2, SnO_2, TiO_2 mixture was weighed to obtain the mixed powder. In order to compensate the volatilization of lead during sintering, 3 mol% PbO was added in the proportioning of raw materials. The raw materials were mixed, and ball milled for 4 h, and then calcined at 850˚C for 2 h in muffle furnace to form the required PLZST perovskite phase. Then, the PLZST powder was mixed with α -Al_2O_3 and ball milled again for 4 h. The highly active powder was dried and screened by filter screen. The sifted powders, appropriate solvent and binder were mixed, and ball milled again. Thick films were obtained by casting machine. The thick films were laminated and isostatically pressed at 65°C and 6000 psi for 20min to ensure uniformity of density, and then cut into regular square piece. Green samples were sintered at 1200 ˚C for 0.5 h.

The sintering temperature was determined by Thermogravimetric differential scanning calorimetry (TG-DSC). X-ray diffraction (XRD, Bede QC200) were detected from 20°to 80°to verify the crystalline phases. The samples scanning electron microscope image (SEM, FEI Inspect-F, Netherlands) were measured to analyze microstructure characteristics of samples. The element components of the samples were analyzed by energy-dispersive spectrometer (EDS).

In order to facilitate the subsequent test of the dielectric properties, the two sides of polished sample were coated with silver paste and sintered at 850 ˚C for the formation of silver electrode. The dielectric constant and dielectric loss were measured using LCR meters (6500P, Wayne Kerr, UK) from room temperature to 300 ˚C at 100 Hz, 1 kHz, 10 kHz and 1 MHz. The polarization–electric field (P–E) hysteresis loops were measured at room temperature and 100 Hz using a ferroelectric tester (RADIANT Precision LC, USA) with high voltage power supply. The energy density is given by: $J = \int EdP$, where E is the applied field, P is the polarization.

3. Results And Discussion

The sintering temperature can be determined by DSC in Fig. 1. The ceramic powder was evenly spread into a uniform thin layer at the bottom of the crucible. In the dynamic atmosphere of nitrogen, the gas flow was 20 mL/min, and the temperature rose from room temperature to 1300 ˚C at a heating rate of 10 ˚C /min. The endothermic peak around 880 ˚C is due to the dissolution of PbO (the melting point of PbO is 886 ˚C). In the range of 1000 ~1150 ˚C, there are many exothermic peaks and obvious weight loss, indicating that the ceramics begin to react and crystallize within this temperature range. There is an endothermic peak near 1300 ˚C, and a lot of weight loss phenomenon. Combined with the analysis of the actual sintering process, the temperature is too high that the ceramics appear over melting phenomenon. Therefore, the sintering temperature range of ceramics was determined to be 1150 ~1200 ˚C.

In Fig. 2(a), the main crystalline phase of all samples is perovskite structure((ICSD-89-8012). And no obvious impurity phase was found, which means the addition of appropriate amount of PbO can offset

the dissolution of PbO in sintering process and maintain the pure perovskite structure. In Fig. 2(b), the diffraction peak near 44°was split into two diffraction peaks of (200) and (002), indicating that all samples are orthonormal phase. Compared with the undoped material, the intensity of the diffraction peak of the composite sample is higher, indicating that the crystallinity is higher. It can be predicted that the sample structure becomes denser. There is no obvious offset in the diffraction peak, so it can be inferred that Al^{3+} does not enter the main lattice of perovskite structure in large quantity, and Al_2O_3 is mainly distributed in the grain gap.

Figure 3 shows the surface microscopic morphology of the samples sintered in lead-free atmosphere and lead atmosphere respectively. Obviously, sintered in lead atmosphere, samples have lower porosity and higher density characteristics. However, there are still a few holes on the surface of all samples, which are caused by the inevitable volatility of lead. The average grain size of all samples is less than 3μm, and the density is increased as the composition of Al_2O_3 increases. This is particularly evident in the sample with x= 0.08(Figure 3(d, h)). With the increase of composite concentration Al_2O_3, there are more and more flake structure at grain spacing.

Figure 4 shows Al_2O_3 doping in PLZST materials and the EDS element distribution of the composite ceramic sample x=0.1. The collection point is located near the grain gap (Figure 4(b)). Thus, the area with pores has no element distribution. The distribution of Pb (Figure 4(c)), Zr (Fig. 4d), and O (Figure 4(e)) on the grain is relatively uniform, mainly came from pre-sintered perovskite structure PLZST. However, the distribution of Al element (Figure 4(f)) is uneven. A small part of Al element distributed in PLZST grain. Most Al elements are enriched in a horizontal line, corresponding to the flake in the SEM image in Figure 4(b). According to the XRD results above, although aluminum atoms are not involved in the phase formation of perovskite structure, but Al_2O_3 exists in the grain gap in the form of flake structure, effectively restraining abnormal grain growth. As can be seen from the Figure 4(a), Al_2O_3 realizes denser and smaller grain size PLZST materials.

Figure 5(a-f) show that the permittivity of all samples increases first and then decreases slowly with increasing temperature and reach the maximum value near Curie temperature (Tc). The two temperature platforms in the intermediate temperature curve are typical orthogonal opposite ferroelectric temperature transformation curves. The ortho phase changes from normal temperature to tetragonal antiferroelectric phase and then to cubic paramagnetic phase[23, 24]. The Curie temperature peak region of all samples is relatively broad. The contrast between samples x=0.01~0.03 and samples x=0, 0.04, 0.08 indicates that the proper combination of Al_2O_3 can delay the temperature relaxation phenomenon of PLZST. The dielectric constant of composite Al_2O_3 samples decreases since the Al_2O_3 has a low dielectric constant (~10). And the change value of ε is less than 500, which is beneficial to improve the temperature stability of ceramic materials. The dielectric loss increases during the heating process, which is mainly due to the relaxation loss. With the increase of Al_2O_3 composite amount, the loss of ceramic sample becomes stable at high temperature, indicating Al_2O_3 composite is beneficial to improve the thermal stability at high frequency. But with the increase of composite amount, the loss also increases. Figure 5(g) shows

the dielectric spectrum at room temperature. With the increase of alumina compound amount, the peak value of dielectric constant decreases from 200 at x=0 to 125 at x=0.1. At the same time, the permittivity is stable within the frequency range of 100 Hz~1MHz. The change of Al_2O_3 compound amount has little effect on dielectric loss. Dielectric loss of all samples is less than 0.025 below 1 MHz.

Figure 6(b) and (c) show the energy storage parameters of each sample based on data collected from Figure 6(a) P-E loop results. In Figure 6(b), all composite samples show an increase in BDS compared to the base material. BDS increased from 16.04 kV/mm at x=0 to 25.57 kV/mm at x =0.02, and BDS increased by 60%. However, BDS decreased as x continue to increase, which is corresponding to other studies[19, 20, 22]. An excessive addition of Al_2O_3 will lead to more Al_2O_3 crystallites (confirmed in Fig. 3(g), (h) and Fig. 4(b)), causing the failure of the microstructure to be completely grown into ceramics. The maximum polarization intensity P_{max} has the same trend as BDS. P_{max} is 4.9 μC/cm^2 at x=0 and 26.2 μC/cm^2 at x=0.02. When the compound content is more than 0.03, P_{max} decreases obviously. This means the increased BDS can't make the polarization intensity reach the saturation intensity. In addition, when x=0.1, BDS and Pmax curves no longer fit. It can be inferred that the dielectric constant drops from 200 to 125 due to excessive Al_2O_3. At the end of the curve, the maximum polarization intensity finally reaches the saturation polarization intensity of the material.

In Fig. 6(c), for x=0, 0.01, 0.02, the maximum energy storage density W_{st} is 0.51, 1.92 and 4.92 J/cm^3, and the effective energy storage density W_{re} is 0.32, 1.15 and 2.95J/cm^3. The energy storage efficiency of all samples fluctuates around 60%. The performance of doped PLZST is generally better than pure PLZST. In the range of x =0.01-0.03, the performance is improved. And at x=0.02, the performance is improved the most. The energy storage efficiency is generally not high, less than 65%. The composite ceramics has the potential to be applied to high energy storage density dielectric ceramics, but it needs to improve the low energy storage efficiency.

4. Conclusion

The (1-x) PLZST–xAl_2O_3 (x=0.0-0.1) ceramic were synthesized by using the conventional solid-state reaction process. The microstructure, dielectric and energy storage properties have been investigated in detail. The test results show that Al_2O_3 is mainly filled in the grain gaps with a flaky structure, which constrain the growth of grain size and increase the density of ceramics. The maximum value of BDS at a composite amount of 0.02 is 25.27 kV/mm, which is 60% higher than that of undoped, and the maximum releasable energy storage density reaches 2.95 J/cm³. While the composite amount exceeds 0.03, related energy storage property decreases. The energy storage efficiency of each sample is generally not high, all of which are less than 65%. It needs to improve the low energy storage efficiency.

Declarations

Acknowledgments

The authors grateful acknowledge the support from the Natural Science Foundation of China (grant no. 51602037) and the Open Foundation of State Key Laboratory of Electronic Thin Films and Integrated Devices (KFJJ201510).

References

1. H.G. Wisken, F. Podeyn, T.H.G.G. Weise, High energy density capacitors for ETC gun applications, IEEE Transactions on Magnetics 37(1) (2001) 332–335.
2. H.G. Wisken, T.H.G.G. Weise, Critical components for high energy density capacitor modules, IEEE Transactions on Magnetics 39(1) (2003) 446–450.
3. X.H. Hao, A review on the dielectric materials for high energy-storage application, Journal of Advanced Dielectrics 03 (2013) 1330001.
4. A.K. N. Ortega, J.F. Scott, B.C. Douglas, M. Tomazawa, K. Shalini, D.G.B. Diestra, R.S. Katiyar, Relaxor-ferroelectric superlattices: high energy density capacitors, Journal of Physics: Condensed Matter 24(44) (2012) 445901.
5. S. Jiang, L. Zhang, G. Zhang, S. Liu, J. Yi, X. Xiong, Y. Yu, J. He, Y. Zeng, Effect of Zr:Sn ratio in the lead lanthanum zirconate stannate titanate anti-ferroelectric ceramics on energy storage properties, Ceramics International 39(5) (2013) 5571–5575.
6. K. Yao, S. Chen, M. Rahimabady, M.S. Mirshekarloo, S. Yu, F.E.H. Tay, T. Sritharan, L. Lu, Nonlinear dielectric thin films for high-power electric storage with energy density comparable with electrochemical supercapacitors, IEEE transactions on ultrasonics, ferroelectrics, and frequency control 58(9) (2011) 1968–74.
7. Prateek, V.K. Thakur, R.K. Gupta, Recent Progress on Ferroelectric Polymer-Based Nanocomposites for High Energy Density Capacitors: Synthesis, Dielectric Properties, and Future Aspects, Chemical Reviews 116(7) (2016) 4260–4317.
8. G. Zhang, D. Zhu, X. Zhang, L. Zhang, J. Yi, B. Xie, Y. Zeng, Q. Li, Q. Wang, S. Jiang, S. Zhang, High-Energy Storage Performance of $(Pb_{0.87}Ba_{0.1}La_{0.02})(Zr_{0.68}Sn_{0.24}Ti_{0.08})O_3$ Antiferroelectric Ceramics Fabricated by the Hot-Press Sintering Method, Journal of the American Ceramic Society 98(4) (2015) 1175–1181.
9. Z. Liu, X. Chen, W. Peng, C. Xu, X. Dong, F. Cao, G. Wang, Temperature-dependent stability of energy storage properties of $Pb_{0.97}La_{0.02}(Zr_{0.58}Sn_{0.335}Ti_{0.085})O_3$ antiferroelectric ceramics for pulse power capacitors, Applied Physics Letters 106(26) (2015) 262901.
10. Q.F. Zhang, Z. Xiao, X.C. Wang, T.Q. Yang, J.F. Wang, S.C. Chen, X. Yao, Effect of excess PbO on the microstructures and electric field induced strain of $Pb_{0.97}La_{0.02}(Zr_{0.63}Sn_{0.26}Ti_{0.11})O_3$ antiferroelectric ceramics, Functional Materials Letters 07(01) (2014) 1350072.
11. X.Z. B.J. Chu, B. Neese, Q.M. Zhang, F. Bauer, Relaxor ferroelectric poly (vinylidene fluoride-trifluoroethylene-chlorofluoroethylene) terpolymer for high energy density storage capacitors, IEEE Transactions on Dielectrics and Electrical Insulation 13 (2006) 1162–1169.

12. J.F. Wang, T.Q. Yang, S.C. Chen, G. Li, High energy storage density performance of Ba, Sr-modified lead lanthanum zirconate titanate stannate antiferroelectric ceramics, Materials Research Bulletin 48(10) (2013) 3847–3849.
13. D.D. N. Setter, L. Eng, G. Fox, S. Gevorgian, S. Hong, A. Kingon, N.Y.P. H. Kohlstedt, G.B. Stephenson, Ferroelectric thin films: review of materials, properties, and applications, J. Appl. Phys. 100 (2006) 46.
14. X.L. Q. Zhang, Y. Zhang, X. Song, J. Zhu, I. Baturin et al., Effect of barium content on dielectric and energy storage properties of (Pb, La, Ba)(Zr, Sn, Ti)O_3 ceramics, Ceramics International 41(2) (2015) 3030–3035.
15. X. Hao, Y. Zhao, S. An, A. Belik, Giant Thermal-Electrical Energy Harvesting Effect of $Pb_{0.97}La_{0.02}(Zr_{0.75}Sn_{0.18}Ti_{0.07})O_3$ Antiferroelectric Thick Film, Journal of the American Ceramic Society 98(2) (2015) 361–365.
16. X. Hao, J. Zhai, L. Kong, Z. Xu, A comprehensive review on the progress of lead zirconate-based antiferroelectric materials, Progress in Materials Science 63 (2014) 1–57.
17. H.Y. Lee, K.H. Cho, H.D. Nam, Grain size and temperature dependence of electrical breakdown in $BaTiO_3$ ceramic, Ferroelectrics 334(1) (2006) 165–169.
18. M. Chen, X. Yao, L. Zhang, Grain size dependence of dielectric and field-induced strain properties of chemical prepared (Pb, La)(Zr, Sn, Ti)O_3 antiferroelectric ceramics, Ceramics International 28(2) (2002) 201–207.
19. A.K. V.S. Puli, R.S. Katiyar, X. Su, C.M. Busta, D.B.Chrisey, M. Tomozawa,, Dielectric breakdown of $BaO–B_2O_3–ZnO–[(BaZr_{0.2}Ti_{0.80})O_3]_{0.85}[(Ba_{0.70}Ca_{0.30})TiO_3]_{0.15}$ glass-ceramic composites, Journal of Non-Crystalline Solids 358(24) (2012) 3510–3516.
20. H. Wang, M. Cao, M. Liu, H. Hao, Z. Yao, H. Liu, Enhanced energy storage properties of fine-crystalline $Ba_{0.4}Sr_{0.6}TiO_3$ ceramics by coating powders with $B_2O_3–Al_2O_3–SiO_2$, Journal of Alloys and Compounds 826 (2020).
21. X. Wang, Y. Zhang, X. Song, Z. Yuan, T. Ma, Q. Zhang, C. Deng, T. Liang, Glass additive in barium titanate ceramics and its influence on electrical breakdown strength in relation with energy storage properties, Journal of the European Ceramic Society 32(3) (2012) 559–567.
22. C. Li, M. Yao, W. Gao, X. Yao, High breakdown strength and energy density in antiferroelectric PLZST ceramics with Al_2O_3 buffer, Ceramics International 46(1) (2020) 722–730.
23. X. Qi, H. Chen, B. Deng, J. Zhao, M. Wei, L. Gao, J. Zhang, Energy-storage properties of Sr-doped PLZST bulk ceramics and thick films, Journal of Materials Science: Materials in Electronics 30(19) (2019) 17916–17922.
24. S. Zou, J. Zhang, L. Gao, J. Zhao, H. Chen, Energy storage properties of PLZST ceramics with tetragonal/orthorhombic two-phase coexistence, Materials Science and Engineering: B 273 (2021).

Figures

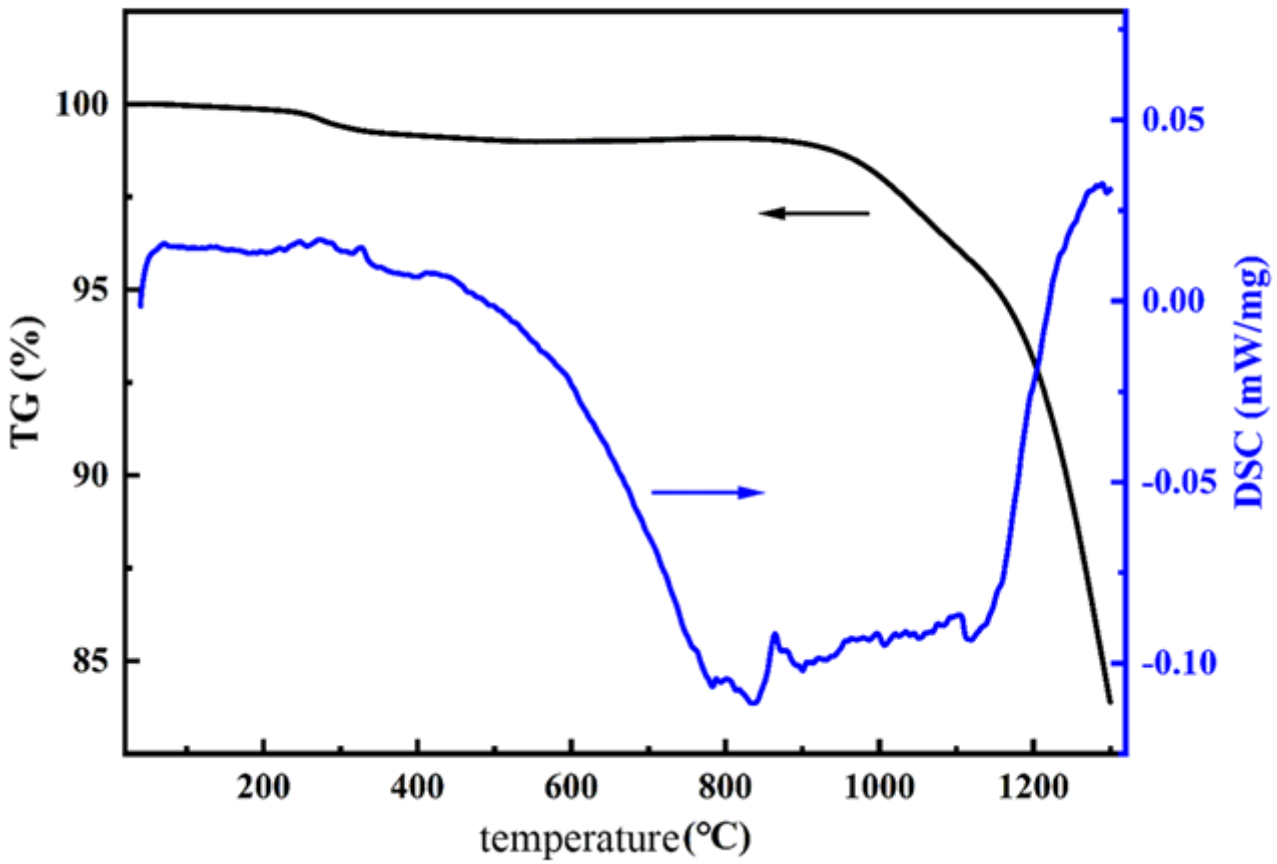

Figure 1

TG-DSC curves from room temperature to 1300 ˚C.

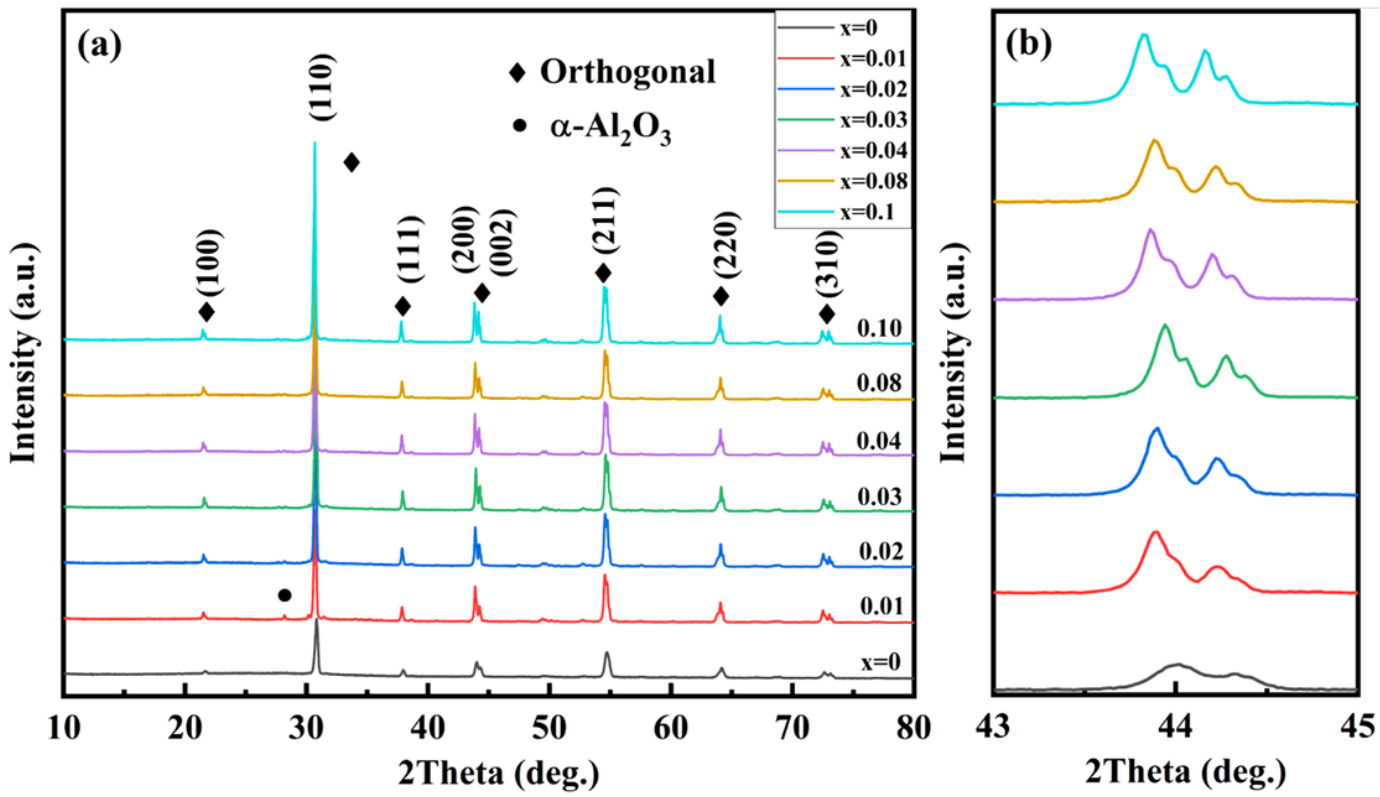

Figure 2

XRD diffraction patterns and local magnification at 43°~45°.

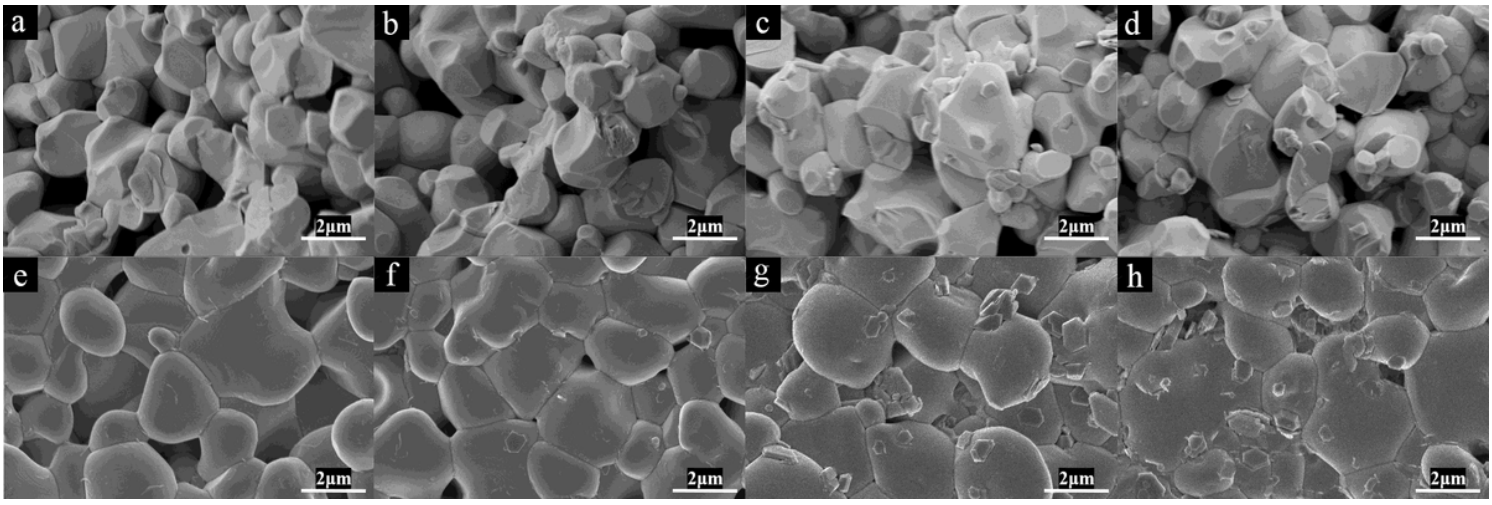

Figure 3

SEM morphology of sample surface in lead-free atmosphere (a)x=0.01; (b) x = 0.03; (c) x = 0.04; (d) x = 0.08; in lead atmosphere (e)x=0.01; (f) x = 0.03; (g) x = 0.04; (h) x = 0.08.

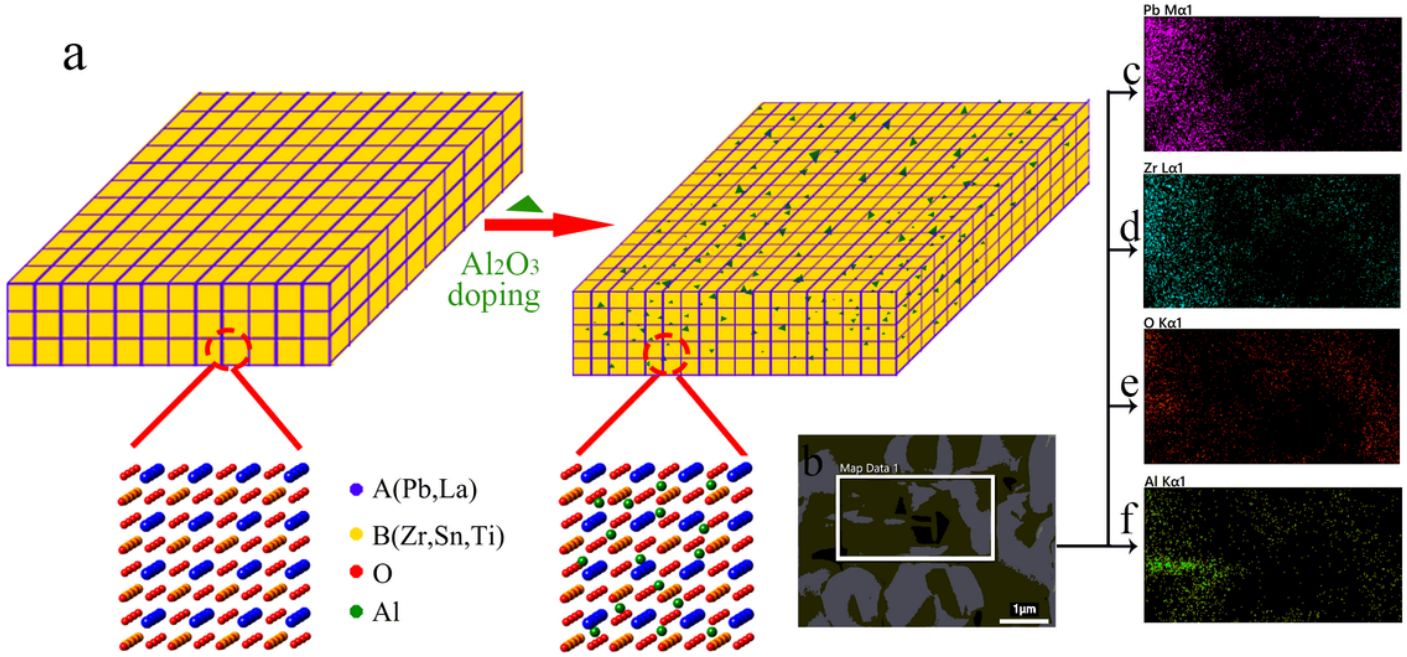

Figure 4

(a)Al2O3 doping PLZST materials model; (b) the collection point morphology of the sample with x=0.01; element distribution by EDS (c) Pb; (d) Zr; (e) O; (f) Al.

Figure 5

Dielectric property curve of composite Al2O3 thick film samples with temperature and frequency (a)x=0; (b) x = 0.01; (c) x = 0.02; (d) x = 0.03; (e) x = 0.04; (f) x = 0.08; (g) all samples at room temperature from 100 Hz to 1 MHz.

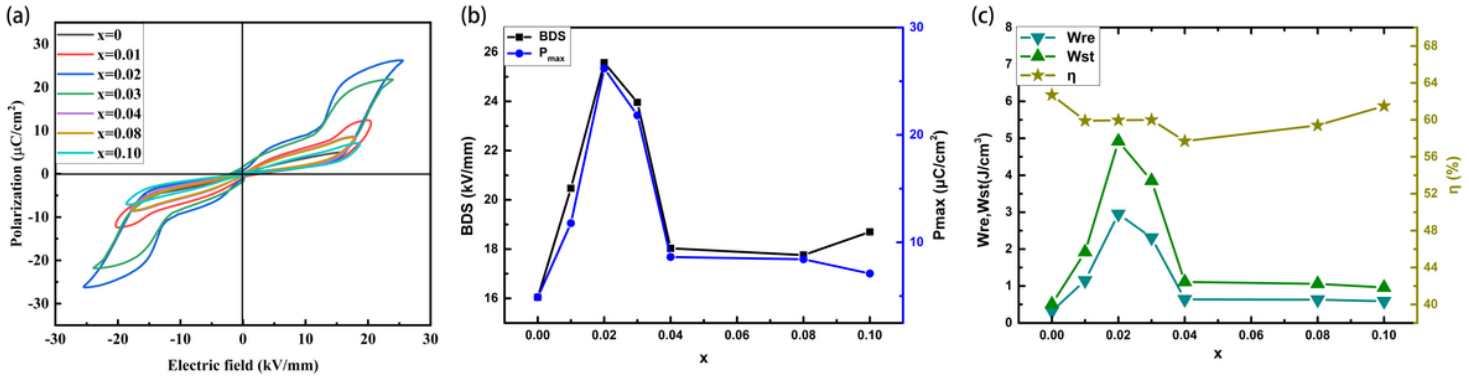

Figure 6

(a) P-E loop of each sample; (b) BDS and Pmax of each sample; (c) Wre, Wst and η of each sample.

Supplementary Files

This is a list of supplementary files associated with this preprint. Click to download.

- graphicalabstract.tif